2017 IEEE 56th Annual Conference on Decision and Control (CDC)
December 12-15, 2017, Melbourne, Australia

Data-driven parameter estimation for optimal connected cruise control

Jin I. Ge and Gábor Orosz

***Abstract*— In this paper we propose a data-based algorithm to identify parameters in a human car-following model, in order to facilitate the implementation of connected cruise control in real traffic. We first present a four-car experiment where the trajectory of each vehicle is recorded. Using the experimental data we identify the car-following parameters for each driver. Using the mean values of human parameters, we implement an optimal connected cruise controller on the last vehicle in the four-car string. We demonstrate by numerical simulation that the optimal connected vehicle design based on human parameter estimation has much smaller variations in headway and velocity, and acceleration compared with the human driver.**

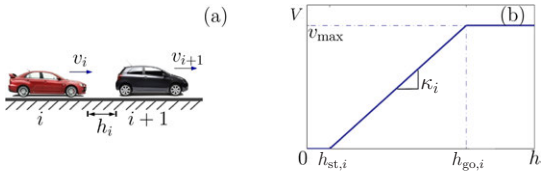

Fig. 1. (a): Single-lane car-following of human-driven vehicles showing the headway and the velocities. (b): The range policy (2) where $v_{\max}$ is the maximum allowed velocity, $h_{\mathrm{st},i}$ is the smallest headway before the vehicle intends to stop, and $h_{\mathrm{go},i}$ is the largest headway after which the vehicle intends to maintain $v_{\max}$.

I. Introduction

Various advanced driver assistance systems have been proposed over the past decades in order to improve road transportation. Specifically, adaptive cruise control (ACC) uses onboard sensors such as radar/lidar to obtain motion information faster and more accurately than human drivers, and provides more adequate commands for the longitudinal motion control [8], [16]. With the availability of affordable wireless communication devices, connected cruise control (CCC) may be used to exploit motion information of vehicles that are beyond the line of sight and undesired acceleration/deceleration can be further suppressed [12]. This may lead to higher road efficiency, less fuel consumption and improved safety in connected vehicle systems.

Existing research on connected vehicle design generally assumes a priori knowledge on the dynamics of preceding vehicles whose signals are used in the connected controller [15], [17], [18]. Such an assumption may not hold as humans may change their behavior in time and vehicles may join and leave the connected vehicle network. Thus, it is necessary to consider online identification of car-following dynamics of preceding vehicles [14]. However, in car-following dynamics, we have to estimate both the feedback gains and the driver reaction time, as the latter has been found to have significant influences on the performance of connected vehicle systems which include human-driven, ACC, and CCC vehicles [3]. While there exist well-developed techniques for parameter identification in systems without time delay [9], estimating the delay time and feedback gains simultaneously is still a challenging problem. The existing researches often have stringent convergence conditions and may only work for fixed parameters [1], [2], [4], [7], [11]. Thus, we need new estimation methods that can be implemented in real time when connected vehicles exchange motion information using dedicated short range communication (DSRC).

Therefore in this paper, we propose a sweeping least square method to simultaneously identify the feedback gains, range policy slope, and driver reaction time of human-driven vehicles, based on headway and velocity data collected via GPS and DSRC. Then, by selecting the mean values of the estimated parameters, we design an optimal connected cruise controller to replace the human driver of the last vehicle in the chain. We show by simulation that the connected cruise controller indeed outperforms the human driver.

The structure of this paper is as follows: in Section II we introduce the car-following behavior of human-driven vehicles. In Section III we introduce the estimation algorithm and use it to estimate the parameters of two drivers in an experiment. In Section IV we present the connected vehicle design and demonstrate the performance of the CCC controller based on the mean parameter values obtained from the estimation. In Section V we reach the conclusion and lay out future works.

II. Describing conventional car-following behavior

In this section we model the car-following behavior of human-driven vehicles in non-emergency situations; see Fig. 1(a). While many existing car-following models [10] can be used to describe the longitudinal behavior of human-driven vehicles, the optimal velocity model has very simple mathematical form and provides great physical intuition. Thus, we choose this to model human-driven vehicles and also use it as a basis for connected vehicle controller.

Based on [6], [12], [13], the optimal velocity model for the human-driven vehicle i is given by

$$\begin{aligned} \dot{h}_i(t) &= v_{i+1}(t) - v_i(t)\,, \\ \dot{v}_i(t) &= \alpha_i\big(V_i(h_i(t-\tau_i)) - v_i(t-\tau_i)\big) \\ &\quad + \beta_i\big(v_{i+1}(t-\tau_i) - v_i(t-\tau_i)\big)\,. \end{aligned} \tag{1}$$

Jin I. Ge and Gábor Orosz are with the Department of Mechanical Engineering, University of Michigan, Ann Arbor, Michigan 48109, USA gejin@umich.edu, orosz@umich.edu

This work was supported by the National Science Foundation (award number 1351456)

Here the dot stands for differentiation with respect to time t, h_i denotes the headway, (i.e., the bumper-to-bumper distance between the vehicle i and its predecessor), and v_i denotes the velocity of vehicle i; see Fig. 1(a). According to (1) the acceleration is determined by two terms: the difference between the headway-dependent desired velocity and the actual velocity, and the velocity difference between the vehicle and its predecessor. The gains α_i and β_i are used to correct velocity errors, while τ_i is the driver reaction time.

The desired velocity is determined by the nonlinear range policy function

$$V_i(h) = \begin{cases} 0 & \text{if} \quad h \le h_{\mathrm{st},i}\,, \\ \kappa_i(h - h_{\mathrm{st},i}) & \text{if} \quad h_{\mathrm{st},i} < h < h_{\mathrm{go},i}\,, \\ v_{\max} & \text{if} \quad h \ge h_{\mathrm{go},i}\,, \end{cases} \tag{2}$$

shown in Fig. 1(b). That is, the desired velocity is zero for small headways ($h \le h_{\mathrm{st},i}$) and equal to the maximum speed $v_{\max}$ for large headways ($h \ge h_{\mathrm{go},i}$). Between these, the desired velocity increases with the headway linearly, with gradient κ_i. Many other range policies may be chosen, but the qualitative dynamics remain similar if the above characteristics are kept [13].

Note that (2) defines the steady-state behavior of vehicle i and, in aggregation, the steady-state traffic flow where vehicles travel with the same constant velocity:

$$h_i(t) \equiv h_i^*\,, \quad v_i(t) \equiv v^* = V_i(h_i^*)\,. \tag{3}$$

In a vehicle string, the equilibrium velocity v^* is determined by the head vehicle while the equilibrium headway h_i^* can be calculated from the range policy (2).

While (h^*, v^*) can be deduced from aggregated traffic data, there has been few research in the past investigating the distribution and variation of parameters α_i, β_i, κ_i, τ_i for individual drivers. However, as geolocation, inertial measurement units and wireless communication devices become less expensive and more widespread, the time is ripe for such investigations. In particular, there may be significant benefits for connected vehicle designs.

III. Car-following parameter estimation

In order to identity the gains α_i, β_i, the range policy slope κ_i, and the reaction time τ_i in the optimal velocity model (1), we designed an experiment where a string of four human-driven vehicles run consecutively on a single-lane road; see Fig. 2. Each vehicle was equipped with a Commsignia on-board unit that provides GPS data and vehicle-to-vehicle communication based on DSRC. We record the vehicles' GPS coordinates (latitude ϕ, longitude λ, elevation r) and speed v every 0.1 [s]. Then the Haversine formula

$$d_{ij} = \Big(R + \frac{r_i + r_j}{2}\Big) \times 2\arcsin\sqrt{\sin^2\Big(\frac{\phi_i - \phi_j}{2}\Big) + \cos\phi_i \cos\phi_j \sin^2\Big(\frac{\lambda_i - \lambda_j}{2}\Big)} \tag{4}$$

Fig. 2. The experiment setup: a string of four vehicles on a single-lane road where all vehicles are equipped with GPS and DSRC devices. The test route is a three-mile section of Mast Road near Dexter, MI.

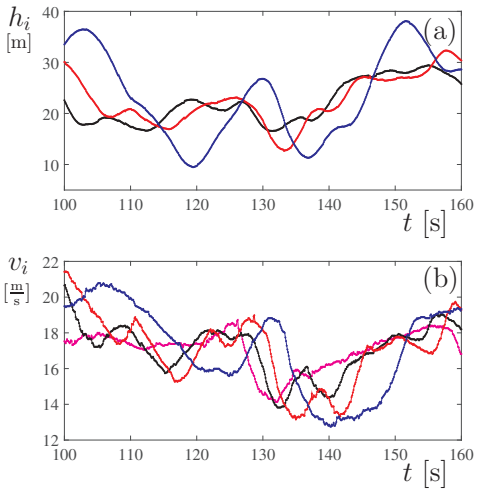

Fig. 3. Headway and velocity profiles of the four-car vehicle string during one test run. The black, red, and blue curves correspond to the headway and velocity of vehicles 3, 2, 1, respectively. The magenta curve in (b) is the velocity of the head vehicle 4.

is used to calculate the great-circle distance d_{ij} between two GPS points (ϕ_i, λ_i, r_i) and (ϕ_j, λ_j, r_j). Here $R = 6371000$ [m] is the nominal radius of the earth.

Thus, the headway for vehicle i is

$$h_i = d_{i(i+1)} - l_i\,, \tag{5}$$

where l_i is the vehicle length. The headway and velocity profiles during one of the test runs are shown in Fig. 3. In Fig. 3(b) we can see that the velocity v_4 of the head vehicle (magenta curve) is almost constant before decreasing at $t \approx 125$ [s], while the velocities of following vehicles 3,2,1 (black, red, and blue curves) start to oscillate before 125 [s] and eventually exhibit more severe deceleration than the head vehicle 1 (magenta curve). This shows that it is difficult for human drivers to suppress the speed fluctuations propagating along the vehicle chain. Such amplifications may not only lead to stop-and-go traffic jams, but can also result in rear-end crashes in heavy traffic.

A connected vehicle is capable to be safer and more efficient as it can suppress such fluctuations by exploiting motion information received from multiple vehicles ahead [18]. However, such a connected controller requires the knowledge of human parameters, so that the human car-following model (1) used in connected cruise control design

matches well with the behavior of preceding vehicles. For example, in order to design a connected cruise controller for the tail vehicle 1, we need to identify parameters α_i, β_i, κ_i and τ_i for vehicles $i = 2, 3$, such that given the velocity v_4 of the head vehicle 4 (magenta curve in Fig. 3(b)), the headway and velocity response of vehicles 3 and 2 (black and red curves in Fig. 3) can be reproduced with minimal mismatches.

A. The sweeping least square method

In order to identify the gains α_i, β_i, the range policy slope κ_i, and the reaction time τ_i, we assume that the GPS and speed data from vehicles i and $i+1$ are available via DSRC. We discretize the second equation in (1) using explicit Euler method with time step $\Delta t = 0.1$ [s]:

$$\begin{aligned} v_i[k+1] - v_i[k] = \Delta t\, \alpha_i \big(\kappa_i h_i[k-m]) - v_i[k-m]\big) \\ + \Delta t\, \beta_i \big(v_{i+1}[k-m] - v_i[k-m]\big)\,. \end{aligned} \tag{6}$$

where $m = \text{round}(\tau_i/\Delta t)$. For simplicity we assume $h_{\text{st},i} = 0$ [m]. However, the least square method will remain valid without this assumption.

We consider N data points over a timespan of $N\Delta t$ and rewrite the unknown parameters α_i, β_i, κ_i in (6) as

$$a = -\alpha_i - \beta_i, \quad b = \alpha_i \kappa_i, \quad c = \beta_i\,. \tag{7}$$

We consider the possible range of driver reaction time $\tau_i \in [\tau_{\min}, \tau_{\max}]$, and sample it such that $\tau_i = m\Delta t$. Then for each m, the least square estimation yields

$$\begin{bmatrix} a(m) \\ b(m) \\ c(m) \end{bmatrix} = (\mathbf{A}^{\mathrm{T}}\mathbf{A})^{-1}\mathbf{A}^{\mathrm{T}}\mathbf{B}(m), \tag{8}$$

where

$$\begin{aligned} \mathbf{A} &= \begin{bmatrix} v_i[1] & h_i[1] & v_{i+1}[1] \\ \vdots & \vdots & \vdots \\ v_i[N] & h_i[N] & v_{i+1}[N] \end{bmatrix}, \\ \mathbf{B}(m) &= \frac{1}{\Delta t} \begin{bmatrix} v_i[m+2] - v_i[m+1] \\ \vdots \\ v_i[m+N+1] - v_i[m+N] \end{bmatrix}, \end{aligned} \tag{9}$$

and the corresponding fitting error is

$$\mathbf{R}(m) = \mathbf{A} \begin{bmatrix} a(m) \\ b(m) \\ c(m) \end{bmatrix} - \mathbf{B}(m)\,. \tag{10}$$

Therefore, we obtain the estimated human reaction time as $\tilde{\tau}_i = \tilde{m}\Delta t$, where

$$\tilde{m} = \arg\min ||\mathbf{R}(m)||_2\,. \tag{11}$$

Correspondingly the estimated human feedback gains are

$$\begin{aligned} \tilde{\alpha}_i &= -a(\tilde{m}) - c(\tilde{m})\,, \\ \tilde{\beta}_i &= c(\tilde{m})\,, \\ \tilde{\kappa}_i &= b(\tilde{m})/\tilde{\alpha}_i\,. \end{aligned} \tag{12}$$

Given reasonable N, each least square calculation (8,9) exhibits a small computational load. Thus, the estimation algorithm (8,9,10,11) can be implemented in real time.

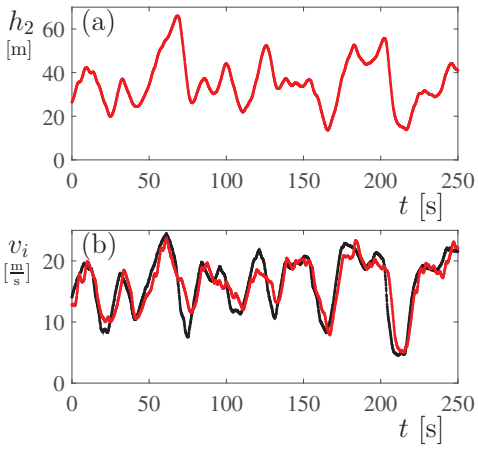

Fig. 4. (a): Headway of vehicle 2 during one test run. (b): Velocity of vehicles 3 (black curve) and 2 (red curve) during one test run.

B. Variations of estimated driver parameters

The estimation algorithm (8,9,10,11) produces the estimation $\tilde{\alpha}_i$, $\tilde{\beta}_i$, $\tilde{\kappa}_i$, $\tilde{\tau}_i$ for each data segment with size N. For example, at time stamp $t_0 = k_0\Delta t$ an estimation is obtained using the motion information $v_i[k]$, $h_i[k]$, and $v_{i+1}[k]$ for $k \in \{k_0 - N, \ldots, k_0 - 1\}$. As the car receives new motion information and the window shifts forward in time, the estimation $\tilde{\alpha}_i$, $\tilde{\beta}_i$, $\tilde{\kappa}_i$, and $\tilde{\tau}_i$ changes. Thus, the estimated parameters will be time-varying.

As an example, we estimate the driver parameters α_2, β_2, κ_2, τ_2 for vehicle 2 using the headway h_2 and the velocities v_2 and v_3 shown in Fig. 4. We consider data length $N = 150$ and human reaction time $0.2 \le \tau_2 \le 2$ [s], that is $m \in \{2, \ldots, 20\}$. The corresponding estimations start at $t = 15$ [s], as shown in Fig. 5. As the data window moves forward in time, the estimated delay time $\tilde{\tau}_2$ varies between $\tau_{\max} = 2$ [s] and $\tau_{\min} = 0.2$ [s], while for most time it stays around 1 [s]. The estimated feedback gains $\tilde{\alpha}$ and $\tilde{\beta}$ are also time-varying. While they are significantly smaller than values previously assumed ($\alpha \approx 0.6$ [1/s], $\beta \approx 0.9$ [1/s]) based on macroscopic data [6], they remain to be positive for most of the time. Since the algorithm for $\tilde{\kappa}_2$ involves division (cf. (12)), we present $\tilde{\kappa}_2$ after filtering the noise using a third-order Savitzky-Golay filter with window size $N\Delta t/2 = 7.5$ [s], see Fig. 5(d).

In Fig. 5, the human reaction time, feedback gains, and range policy slope varies in time. In the simplified case, a connected vehicle design can use their mean values, but it is desirable to examine their distributions over a larger data set.

C. Distributions of estimated driver parameters

As we did multiple test runs and accumulated over 10000 estimations for every driver parameter for vehicles 2, 3, and 4, we are interested in the distributions of those parameters and the difference among human drivers. In particular, we present the distributions of driver parameters for vehicles 2 and 3.

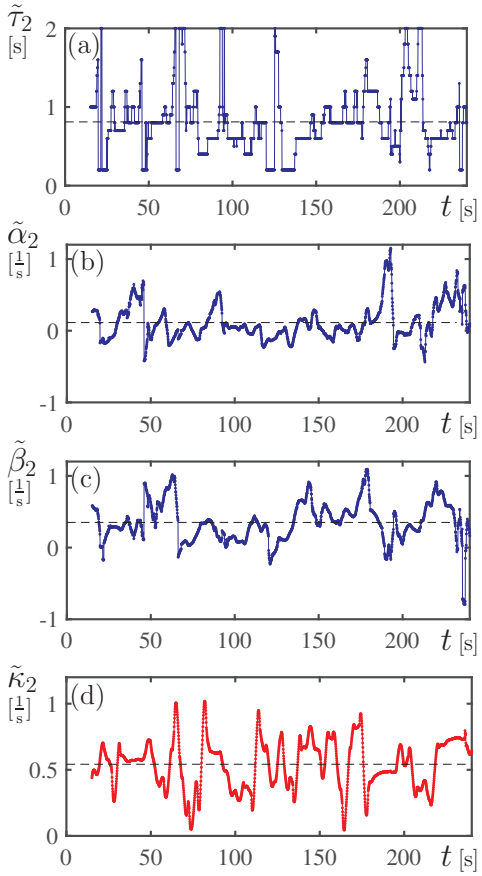

Fig. 5. Estimated driver parameters of vehicle 2 starting from $t = 15$ [s] in a test run. The related headway and velocity information is shown in Fig. 4. (a): The time profile of estimated delay time $\tilde{\tau}_2$ with data window size $N = 150$, quantization step $\Delta t = 0.1$ [s], and the range of possible delay $\tau \in [0, 4]$ [s]. (b,c): The time profile of estimated feedback gains $\tilde{\alpha}_2$, $\tilde{\beta}_2$. (d): The time profile of estimated range policy slope $\tilde{\kappa}_2$ filtered by a third-order Savitzky-Golay filter with window size 7.5 [s]. The dashed black lines are the mean values.

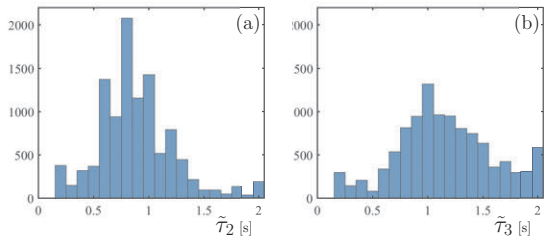

Fig. 6. (a, b) Histogram of estimated driver reaction time for vehicles 2 and 3, respectively.

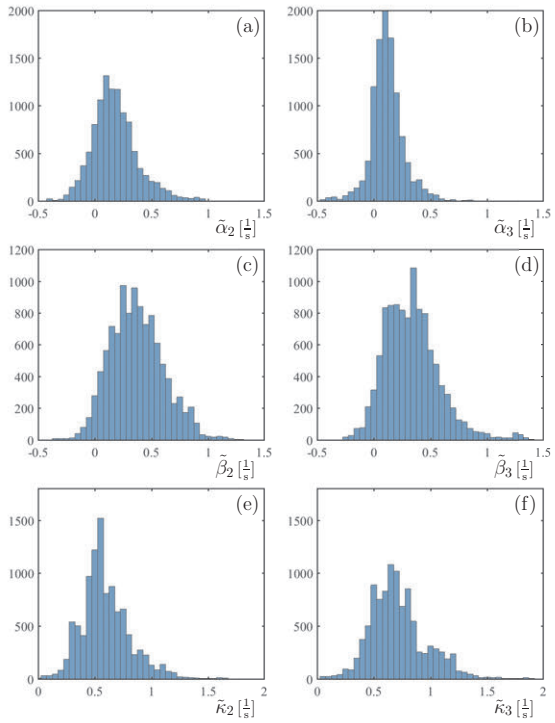

Fig. 7. (a,c,e): Histogram of estimated human feedback gains $\tilde{\alpha}_2$, $\tilde{\beta}_2$ and range policy slope $\tilde{\kappa}_2$ for vehicle 2. (b,d,f): Histogram of estimated human feedback gains $\tilde{\alpha}_3$, $\tilde{\beta}_3$ and range policy slope $\tilde{\kappa}_3$ for vehicle 3.

In Fig. 6(a,b) we show the histogram of estimated driver reaction time $\tilde{\tau}_2$ and $\tilde{\tau}_3$, respectively. It seems that both Gamma and Gaussian distributions could be used to describe the stochasticity of the human reaction time. The mean and variance of the driver reaction time for car 3 is $(1.16, 0.15)$ [s], while for car 2 we have $(0.90, 0.09)$ [s].

It is noted that the driver for vehicle 2 less driving experience compared with the driver for vehicle 3. While a much larger sample is needed to establish the relation between driving proficiency and human car-following parameters, the comparison between Fig. 6(a) and Fig. 6(b) provides some intuition on the variation between different drivers. Note that the experienced driver has smaller and more consistent reaction time, which may lead to more reliable response to the traffic environment. However, the values of mean reaction time are not significantly different for the two drivers, which may be exploited in connected vehicle design.

In Fig. 7 we show the histograms of human feedback gains $\tilde{\alpha}_i$, $\tilde{\beta}_i$ and range policy slope $\tilde{\kappa}_i$ for vehicle 2 (panels (a,c,e)) and vehicle 3 (panels (b,d,f)). In each panel the histogram can be approximated by a Gaussian distribution with different mean and variance. By comparing Fig. 7(a,c,e) and Fig. 7(b,d,f) we can see that while there exist some differences between the histograms, the human feedback gains $\tilde{\alpha}_i$, $\tilde{\beta}_i$ and range policy slope $\tilde{\kappa}_i$ vary in the same range for the two drivers. Thus, it is feasible to use a nominal $\tilde{\alpha}$, $\tilde{\beta}$, $\tilde{\kappa}$ for both drivers in connected vehicle design.

IV. Close-loop verification of estimation algorithm

To verify the effectiveness of the proposed identification algorithm (8,9,10,11), we use the estimated parameters of drivers 2 and 3 to design an optimal connected cruise controller for the tail vehicle 1, so that it utilizes motion information from all three vehicles ahead, see Fig. 8. Then we examine the performance of the connected cruise controller through numerical simulation.

For simplicity, we describe the dynamics of vehicles $i = 2, 3$ using the optimal velocity model with nominal

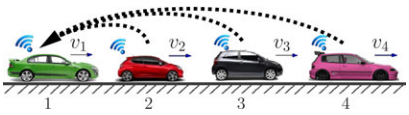

Fig. 8. A string of $3+1$ vehicles in a single-lane scenario. The tail vehicle 1 is driven by a connected cruise controller that uses motion information from human-driven vehicles ahead. Dashed arrows indicate the flow of information used by the connected cruise control.

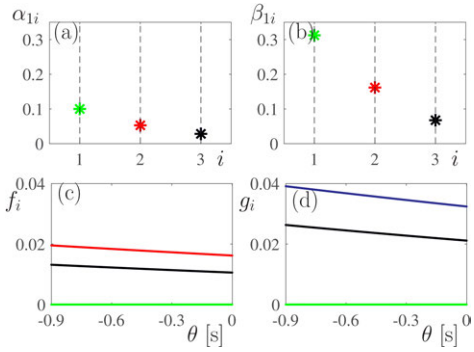

Fig. 9. (a, b): The optimized feedback gains $\alpha_{1i}, \beta_{1i}, i = 1, 2, 3$ of the CCC vehicle in a string of $(3{+}1)$ vehicles. (c, d): The optimized distribution kernels $f_i(\theta), g_i(\theta)$ for the CCC vehicle. The green, red, and black curves correspond to $i = 1, 2, 3$, respectively. The human parameters are $\alpha = 0.2$ [1/s], $\beta = 0.4$ [1/s], $\kappa = 0.6$ [1/s], and $\tau = 0.9$ [s]. The design parameters are $\gamma_1 = 0.01\,[1/\mathrm{s}^2]$, $\gamma_2 = 0.04\,[1/\mathrm{s}^2]$.

parameters $\alpha = 0.2$ [1/s], $\beta = 0.4$ [1/s], $\kappa = 0.6$ [1/s], and driver reaction time $\tau = 0.9$ [s]. However, the algorithm still works for heterogeneous human parameters; see [5]. We assume that the tail vehicle 1 receives motion information from vehicles $2, 3, 4$ every 0.1 [s] and packet drops are negligible. Thus, when the tail vehicle is driven by a CCC controller, its car-following dynamics becomes

$$\begin{aligned} \dot{\tilde{h}}_1(t) &= v_2(t) - \tilde{v}_1(t)\,, \\ \dot{\tilde{v}}_1(t) &= u(t)\,, \end{aligned} \tag{13}$$

where $u(t)$ is the acceleration to be designed using the velocity and headway information obtained via V2V communication, and $\tilde{h}_1$, $\tilde{v}_1$ are the headway and velocity of the tail vehicle equipped with CCC controller.

We define the cost function based on the CCC controller's acceleration and deviations from the uniform flow

$$J(u) = \int_0^{t_\mathrm{f}} \Big(u^2 + \gamma_1 \big(\kappa \tilde{h}_1 - \tilde{v}_1\big)^2 + \gamma_2 \big(v_2 - \tilde{v}_1\big)^2 \Big)\, \mathrm{d}t\,, \tag{14}$$

where $\gamma_1 > 0$, $\gamma_2 > 0$ and the nominal human parameter $\kappa = 0.6$ [1/s] is used so that the connected cruise controller would generate similar behaviors as the human drivers nearby. In (14) the first term is related with the fuel economy of the CCC vehicle, and the latter two terms account for the active safety and traffic efficiency. While other cost functions may be chosen, the quadratic form of (14) allows us to obtain analytical optimal solutions, requiring little computation load and providing great physical intuition.

Using results in [5], the optimal CCC controller is given by

$$\begin{aligned} u(t) = {} & \alpha_{11}\big(\kappa \tilde{h}_1(t) - \tilde{v}_1(t)\big) + \beta_{11}\big(v_2(t) - \tilde{v}_1(t)\big) \\ & + \sum_{i=2}^{3} \Big(\alpha_{1i}\big(\kappa h_i(t) - v_i(t)\big) + \beta_{1i}\big(v_{i+1}(t) - v_i(t)\big) \Big) \\ & + \sum_{i=2}^{3} \int_{-\tau}^{0} f_i(\theta)\big(\kappa h_i(t+\theta) - v_i(t+\theta)\big)\, \mathrm{d}\theta \\ & + \sum_{i=2}^{3} \int_{-\tau}^{0} g_i(\theta)\big(v_{i+1}(t+\theta) - v_i(t+\theta)\big)\, \mathrm{d}\theta\,, \end{aligned} \tag{15}$$

where the optimal feedback gains and kernels are

$$\begin{aligned} &\begin{bmatrix} \alpha_{1i} & \beta_{1i} \end{bmatrix} = \begin{bmatrix} 1 & 1 \end{bmatrix} \mathbf{P}_{1i}, \\ &\begin{bmatrix} f_i(\theta) & g_i(\theta) \end{bmatrix} = \begin{bmatrix} 1 & 1 \end{bmatrix} \mathrm{e}^{\hat{\mathbf{A}}_1(\theta+\tau)} (\mathbf{P}_{1i}\mathbf{B}_1 + \mathbf{P}_{1(i-1)}\mathbf{B}_2)\,, \end{aligned} \tag{16}$$

for $i = 1, 2, 3$. Here $\mathbf{P}_{1i}$ is the decomposed solution of the Riccati equation that corresponds to optimal feedback terms from vehicle i. It can be calculated recursively,

$$\mathrm{vec}(\mathbf{P}_{1i}) = \mathbf{M}^{i-1} \mathrm{vec}(\mathbf{P}_{11})\,, \tag{17}$$

where $\mathrm{vec}(\cdot)$ gives a column vector by stacking the columns of the matrix on the top of each other, and the first block $\mathbf{P}_{11} = \begin{bmatrix} p_{11} & p_{12} \\ p_{12} & p_{22} \end{bmatrix}$ is solely determined by the design parameters γ_1, γ_2 and the range policy parameter κ:

$$\begin{aligned} p_{11} &= \frac{-\gamma_1 + \sqrt{\gamma_1}\sqrt{\gamma_1 + \gamma_2 + 2\kappa\sqrt{\gamma_1}}}{\kappa}\,, \\ p_{12} &= \sqrt{\gamma_1} - p_{11}\,, \\ p_{22} &= -2\sqrt{\gamma_1} + \sqrt{\gamma_1 + \gamma_2 + 2\kappa\sqrt{\gamma_1}} + p_{11}\,. \end{aligned} \tag{18}$$

The matrix in (17) is given by

$$\mathbf{M} = -\big(\mathbf{I} \otimes \hat{\mathbf{A}}_1 + \mathbf{A}_1^{\mathrm{T}} \otimes \mathbf{I} + \mathbf{B}_1^{\mathrm{T}} \otimes \mathrm{e}^{\tau \hat{\mathbf{A}}_1}\big)^{-1} \big(\mathbf{B}_2^{\mathrm{T}} \otimes \mathrm{e}^{\tau \hat{\mathbf{A}}_1}\big)\,, \tag{19}$$

with the coefficient matrices

$$\begin{aligned} &\hat{\mathbf{A}}_1 = \mathbf{A}_1^{\mathrm{T}} - \mathbf{P}_{11}\mathbf{D}_1\mathbf{D}_1^{\mathrm{T}}\,, \\ &\mathbf{A}_1 = \begin{bmatrix} 0 & \kappa \\ 0 & 0 \end{bmatrix},\ \mathbf{B}_1 = -\begin{bmatrix} \alpha & \beta \\ \alpha & \beta \end{bmatrix},\ \mathbf{B}_2 = \begin{bmatrix} 0 & 0 \\ \alpha & \beta \end{bmatrix},\ \mathbf{D}_1 = \begin{bmatrix} -1 \\ -1 \end{bmatrix}. \end{aligned} \tag{20}$$

Note that the first row in the optimal controller (15) can be implemented without connectivity, indicating that when V2V connectivity is lost, the CCC controller degrades to an optimal ACC controller. Based on (16,18), the corresponding feedback gains are

$$\alpha_{11} = \sqrt{\gamma_1}, \quad \beta_{11} = -\sqrt{\gamma_1} + \sqrt{\gamma_1 + \gamma_2 + 2\kappa\sqrt{\gamma_1}}\,. \tag{21}$$

In Fig. 9, we show the optimal feedback gains and kernels of the CCC vehicle 1, when it receives motion information from vehicles $2, 3, 4$, and the car-following dynamics of vehicle $2, 3$ are described by (1) for the human parameters mentioned above. We also use design parameters $\gamma_1 = 0.01\,[1/\mathrm{s}^2]$ and $\gamma_2 = 0.04\,[1/\mathrm{s}^2]$. We can see that the feedback gains and kernels decrease as i increases.

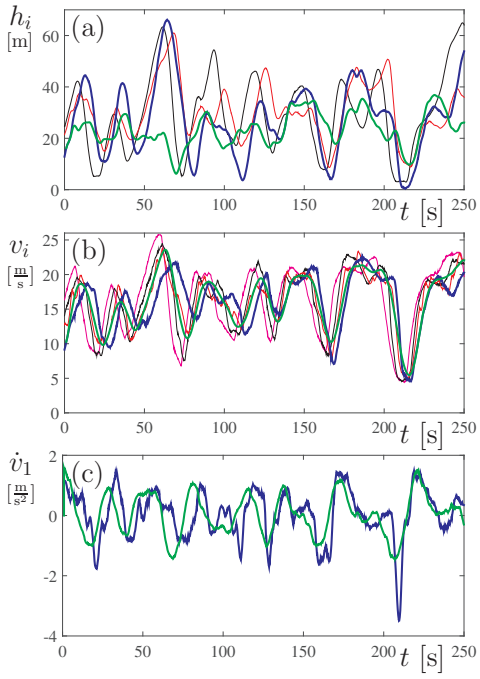

Fig. 10. The headway, velocity, and acceleration profiles of a $(3+1)$-car vehicle string. The color scheme is the same as in Fig. 3. The green curves correspond to the response of the tail vehicle when it is driven by the CCC controller (15).

In order to evaluate the performance of the optimal CCC design, we simulate the motion of the CCC vehicle using the measured headway and velocity of vehicles $2, 3, 4$. In Fig. 10(a) the black, red, and blue curves are the headway h_3, h_2, h_1 observed in the experiment, while the green curve is the headway $\tilde{h}_1$ of the tail vehicle controlled by CCC. We find the CCC vehicle (green curve) has much smaller fluctuations in headway than any human-driven vehicle. While the real tail vehicle 1 almost collided with vehicle 2 in the experiment (at $t \approx 210$ [s], $h_1(t) \approx 0$ [m]), such safety hazard is avoided when the tail vehicle is driven by the CCC. In Fig. 10(b) the magenta curve is the velocity v_1 of the head vehicle, while the other curves have the same color scheme as in panel (a). Again, the tail vehicle will have smaller fluctuations in velocity compared with other vehicles when it is driven by a CCC controller. In Fig. 10(c) we compare the acceleration $\dot{v}_1$ of the tail vehicle (blue curve) and the acceleration u of the CCC vehicle (green curve). Notice that the CCC vehicle reduces harsh braking and acceleration maneuvers. In general the CCC controller demonstrates significant performance improvements compared with human-driven vehicles. The next step for this research is to implement the CCC controller based on real-time parameter estimation on experimental vehicles and test it in real traffic.

V. CONCLUSIONS

In this paper a connected cruise controller has been designed based on real measurement data. We used the position and headway measurements to estimate the range policy, the feedback gains and the reaction time delay simultaneously for the human-driven vehicles ahead by a sweeping least square approach. After identifying the distributions of the human parameters we used their mean values in an optimal connected cruise control design. We demonstrated that the CCC outperformed the human drivers and reduced the unwanted oscillations in the system.

ACKNOWLEDGMENT

The authors thank Professor A. Galip Ulsoy for the very insightful discussions. We also thanks the Commsignia, Inc. for their generous technical support.

REFERENCES

[1] S. Diop, I. Kolmanovsky, P. Moraal, and M. V. Nieuwstadt, "Preserving stability/performance when facing an unknown time-delay," *Control Engineering Practice*, vol. 9, no. 12, pp. 1319–1325, 2001.

[2] S. Drakunov, W. Perruquetti, J.-P. Richard, and L. Belkoura, "Delay identification in time-delay systems using variable structure observers," *Annual Reviews in Control*, vol. 30, no. 2, pp. 143–158, 2006.

[3] J. I. Ge and G. Orosz, "Dynamics of connected vehicle systems with delayed acceleration feedback," *Transportation Research Part C*, vol. 46, pp. 46–64, 2014.

[4] ——, "Estimation of feedback gains and delays in connected vehicle systems," in *Proceedings of the American Control Conference*. IEEE, 2016, pp. 6000–6005.

[5] ——, "Optimal control of connected vehicle systems with communication delay and driver reaction time," *IEEE Transactions on Intelligent Transportation Systems*, vol. 18, no. 8, pp. 2056–2070, 2017.

[6] J. I. Ge, G. Orosz, D. Hajdu, T. Insperger, and J. Moehlis, "To delay or not to delay - stability of connected cruise control," in *Time Delay Systems - Theory, Numerics, Applications and Experiments, Advances in Delays and Dynamics*, G. Orosz, T. Ersal, and T. Insperger, Eds., vol. 7. Springer, 2016, pp. 263–282.

[7] O. Gomez, Y. Orlov, and I. V. Kolmanovsky, "On-line identification of SISO linear time-invariant delay systems from output measurements," *Automatica*, vol. 43, no. 12, pp. 2060 – 2069, 2007.

[8] P. A. Ioannou and C. C. Chien, "Autonomous intelligent cruise control," *IEEE Transactions on Vehicular Technology*, vol. 42, no. 4, pp. 657–672, 1993.

[9] P. A. Ioannou and J. Sun, *Robust Adaptive Control*. Dover Publications, 2012.

[10] K. Nagel, P. Wagner, and R. Woesler, "Still flowing: Approaches to traffic flow and traffic jam modeling," *Operations Research*, vol. 51, no. 5, pp. 681–710, 2003.

[11] Y. Orlov, L. Belkoura, J.-P. Richard, and M. Dambrine, "Adaptive identification of linear time-delay systems," *International Journal of Robust and Nonlinear Control*, vol. 13, pp. 857–872, 2003.

[12] G. Orosz, "Connected cruise control: modeling, delay effects, and nonlinear behavior," *Vehicle System Dynamics*, vol. 54, no. 8, pp. 1147–1176, 2016.

[13] G. Orosz, R. E. Wilson, and G. Stépán, "Traffic jams: dynamics and control," *Philosophical Transactions of the Royal Society A*, vol. 368, no. 1928, pp. 4455–4479, 2010.

[14] R. Pandita and D. Caveney, "Preceding vehicle state prediction," in *2013 IEEE Intelligent Vehicles Symposium*, 2013, pp. 1000–1006.

[15] W. B. Qin, M. M. Gomez, and G. Orosz, "Stability and frequency response under stochastic communication delays with applications to connected cruise control design," *IEEE Transactions on Intelligent Transportation Systems*, vol. 18, no. 2, pp. 388–403, 2017.

[16] P. Seiler, A. Pant, and K. Hedrick, "Disturbance propagation in vehicle strings," *IEEE Transactions on Automatic Control*, vol. 49, no. 10, pp. 1835–1842, 2004.

[17] M. Wang, W. Daamen, S. P. Hoogendoorn, and B. van Arem, "Rolling horizon control framework for driver assistance systems. part I: Mathematical formulation and non-cooperative systems," *Transportation Research Part C: Emerging Technologies*, vol. 40, pp. 271 – 289, 2014.

[18] L. Zhang and G. Orosz, "Motif-based analysis of connected vehicle systems: delay effects and stability," *IEEE Transactions on Intelligent Transportation Systems*, vol. 17, no. 6, pp. 1638–1651, 2016.